

Supporting Information

Layered $\text{H}_{0.68}\text{Ti}_{1.83}\text{O}_4$ /Reduced Graphene Oxide Nanosheets Cathode for High Performance Rechargeable Magnesium Batteries

Chengcheng Chen,^{†, ‡, §} Jianchao Sun,^{+, §} Licheng Miao,[†] Zhenhua Yan,^{*, †} and Jun Chen[†]

[†] Key Laboratory of Advanced Energy Materials Chemistry (Ministry of Education), Renewable Energy Conversion and Storage Center, College of Chemistry, Nankai University, Tianjin 300071 (China)

[‡] China Electronic Product Reliability and Environmental Testing Research Institute (CEPREI), Guangzhou 510610, China

[§] School of Environmental and Materials Engineering, Yantai University, Yantai 264000, Shandong, China.

Table of Contents

Experimental Section

Material Synthesis

Electrolyte Preparation

Material Characterization

Electrochemical Measurement

Density functional theory calculations

Ab initio Molecular Dynamics

Figure S1-S16

Table S1

Experimental Section

Material Synthesis



All the chemicals were of reagent grade including Rutile TiO_2 and Cs_2CO_3 (99.9% purity). The layered $H_{0.68}Ti_{1.83}O_4 \cdot xH_2O$ were synthesized by conventional high-temperature calcination and following ion exchange. Typically, a stoichiometric of Cs_2CO_3 and TiO_2 (molar ratio of $Cs_2CO_3:TiO_2=0.34:1.83$) was uniformly mixed *via* a solution-evaporation method. Then, the $Cs_{0.68}Ti_{1.83}O_4$ were obtained by heating the compounds at $800^\circ C$ for 12 h in air. The interlayers Cs^+ were extracted through intensely stirring 2 g $Cs_{0.68}Ti_{1.83}O_4$ in 20 mL HCl solution (1 M) for various hours (20, 40, 60 and 80 h) to obtain products with different protonation level. Notably, HCl solution was renewed every 10 h. After high speed centrifugation, the $H_{0.68}Ti_{1.83}O_4 \cdot xH_2O$ product were obtained.

Exfoliated $H_{0.68}Ti_{1.83}O_4 \cdot xH_2O$ loading on rGO nanosheets.

A weight of 0.3-0.5 g $H_{0.68}Ti_{1.83}O_4 \cdot xH_2O$ (HTO) powder was evenly dispersed into 20 mL aqueous solution with 2 mL tetrabutylammonium hydroxide aqueous solution (60 % TBAOH), which could strip the few layers off the bulk architecture and produce the stable colloidal suspensions. The solution was strongly stirring (600 rpm) for 3 days at room temperature. The resulting dispersion was obtained from supernatant via high speed centrifugation. Then, moderate reduced graphene oxides (RGO) nanosheets (prepared via modified Hummer method) were mixed into the translucent solution to adsorb few-layered HTO lamellas through ultrasound (1 h) and stirring (1 days). The final sample was collected by centrifugation and heated at $150^\circ C$ for 2 h in Ar at tube furnace to remove surface water.

Electrolyte Preparation

APC electrolyte

Electrolytes were prepared in the glovebox under pure argon atmosphere (<1 ppm of water and oxygen). The 0.25 M "all phenyl" complex (APC) salt solutions were synthesized by reaction between aluminum chloride ($AlCl_3$, Alfa Aesar, ultra-dry 99.99 %) dissolved in THF (anhydrous, 99.9 %) and phenyl magnesium chloride (PhMgCl, Alfa Aesar, 2 M solution in THF) as follows: (1) a certain amount of $AlCl_3$ powder was slowly dropped into THF under vigorous stirring, followed stirring for 12 h. (2) The as-prepared $AlCl_3/THF$ solution was slowly added into a proportionable amount of 2 M PhMgCl/THF solution (molar ratio of $AlCl_3: PhMgCl = 1: 2$) with vigorous stirring for 12 h. Thus, the APC electrolyte was prepared including 0.25 M of Mg_2Cl^{3+} cations and $AlPh_2Cl^{2-}$ anions in THF.

Material Characterization

The structure and morphology of samples were measured by powder X-ray diffraction (XRD, Rigaku MiniFlex600, Cu K α radiation, $\lambda=1.54056$ Å), field-emission scanning electron microscopy (SEM, JEOL JSM-7500F, 5 kV), and transmission electron microscopy (TEM, Philips Tecnai FEI, 200 kV). Raman spectra were obtained on a confocal Raman microscope (DXR, Thermo-Fisher Scientific) with an argon-ion laser ($\lambda=532$ nm) in ambient air. The specific surface areas of the resultant products were investigated by nitrogen adsorption–desorption measurements using a NOVA 2200e analyzer. The electronic states of electrodes were investigated by XPS (PHI 5000 Versa Probe). Inductively coupled plasma-atomic emission spectroscopy (ICP-AES, PerkinElmer Optima 8300) and Energy Dispersive X-ray Detector (EDX, JEOL JSM-7500F) were used to analyze composition of the electrodes. The X-ray absorption near-edge structure spectra (XANES) and extended X-ray absorption fine structure (EXAFS) were collected on BL14W1 beamline of Shanghai Synchrotron Radiation Facility (SSRF) and analyzed with software of Athena.

Electrochemical Measurement

The electrochemical performance was measured using a two electrode coin-type cell (CR2032) and assembled in an argon-filled glove box. For preparing the working electrodes, a mixture of the samples, Super P, and polyvinylidene fluoride (PVdF) binder at a weight ratio of 7:2:1 were dispersed in N-methyl-2-pyrrolidinone (NMP) solvent and ground thoroughly to form a slurry. Then, the slurry was pasted on pure Ti current collectors and dried at 80 °C for 12 h. The loading density is about 1 mg/cm² in this study. Magnesium ribbons (99.99%) were used as the counter electrodes, the glass fibers were used as separators. Galvanostatic tests and galvanostatic intermittent titration technique (GITT) were run under different current densities between cut off voltages of 0.01-2.00 V (vs. Mg²⁺/Mg) on a CT2001A cell test instrument (LAND Electronic Co.) at room temperature. Cyclic voltammetry (CV) of cells and electrolytes and electrochemical impedance spectroscopy (EIS) were measured on a CHI660E electrochemical work station.

Density functional theory (DFT) calculations of interaction between HTO and graphene

To estimate the interaction between HTO and graphene, the graphene and TiO heterojunction is constructed with a vacuum layer of 15 Å, including a $\sqrt{3} \times 2 \times 1$ graphene supercell and a TiO primitive cell. The 2 x 2 x 2 k-point mesh is applied to optimize this configuration.

Ab initio Molecular Dynamics

Density functional theory (DFT) calculations were performed via Vienna ab initio simulation package (VASP) with Perdew-Burke-Ernzerhof (PBE) generalized gradient approximation (GGA) and projector augmented-wave (PAW) method. The cutting-off energy was set to be 510 eV. All the structures have been fully optimized with the convergence criterion of the total energy (10^{-5} eV/atom) and the residual Hellmann–Feynman force (0.035 eV/Å). Ab initio molecular dynamics (AIMD) was used to evaluate the structural stability and the diffusion capability of Mg^{2+} in $\text{Mg}_{0.5}\text{Ti}_{1.83}\text{O}_4$. The simulations were performed on a $4 \times 1 \times 2$ supercell at 300 K using NVT ensemble (Number of particles, Volume, and Temperature). To avoid the disturbance of the uncertainties, we built the ideal supercell with ignoring the actual crystal water and H^+ . The time step was set to be 1 fs and both simulations last 3000 fs.

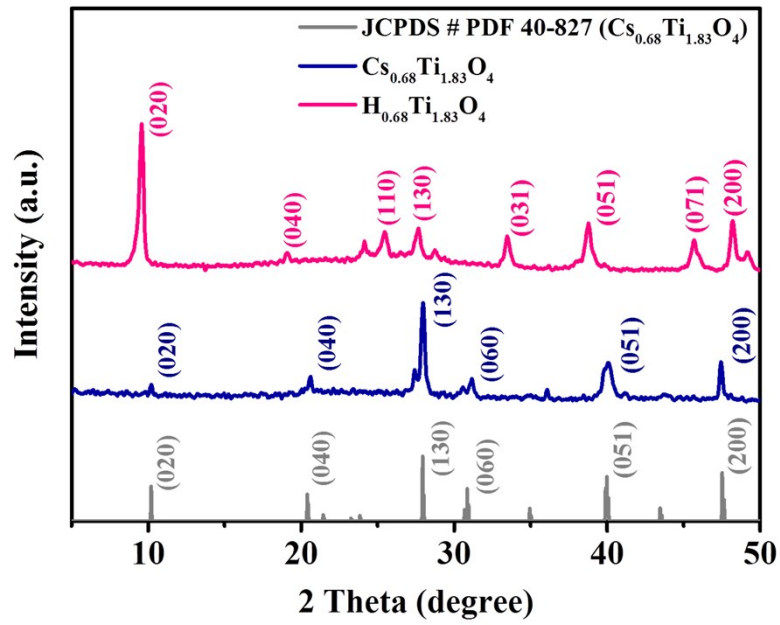


Figure S1. XRD patterns of as-prepared $Cs_{0.68}Ti_{1.83}O_4$ and $H_{0.68}Ti_{1.83}O_4$.

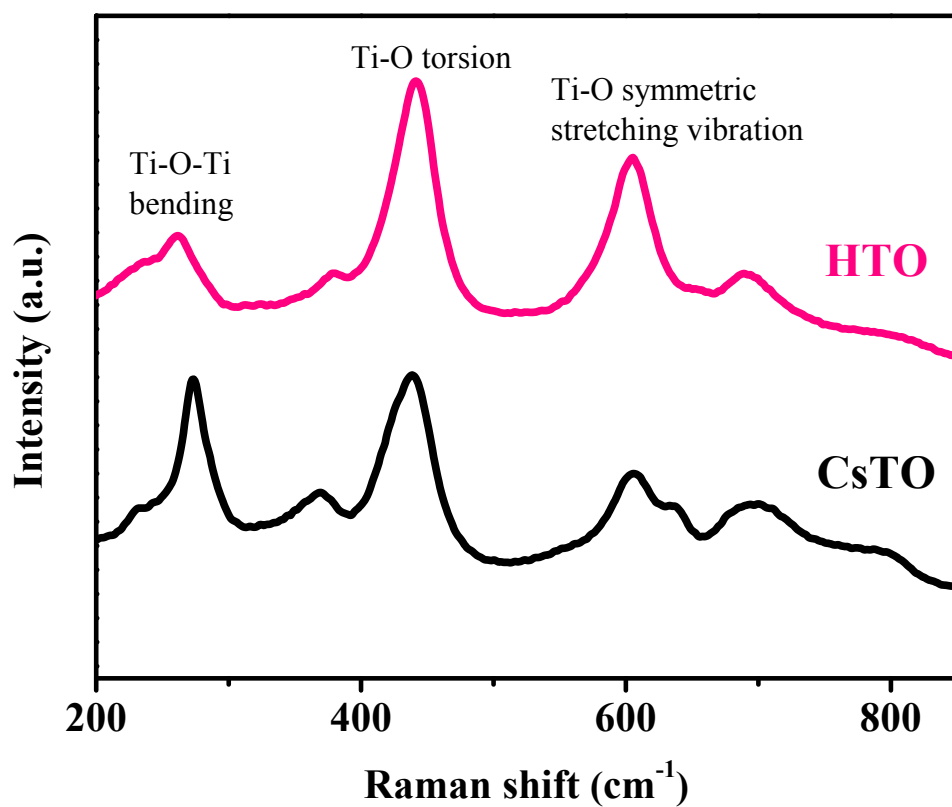


Figure S2. Raman spectrum of as-prepared CTO and HTO. (After protonation, HTO displays the similar Raman peaks with original CTO. This indicates that HTO inherits the straight Ti-O layered structure of CTO.)

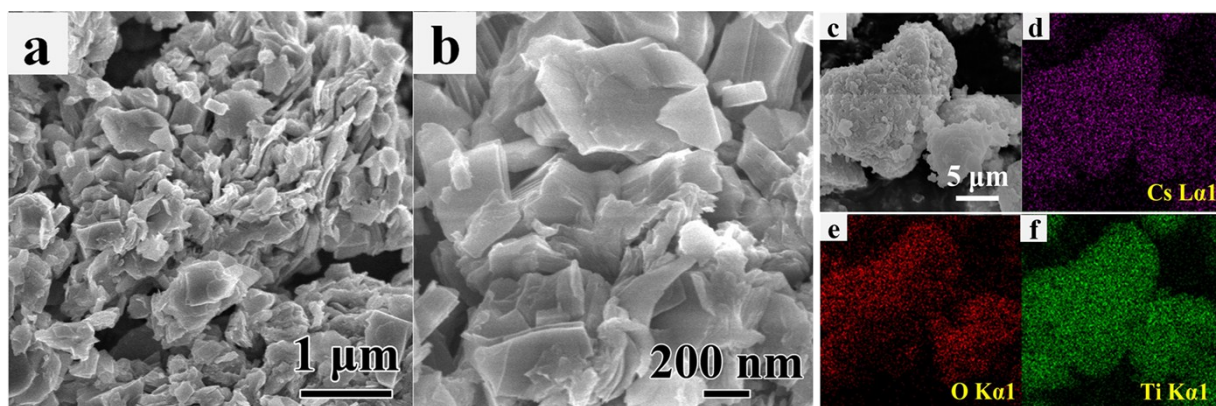


Figure S3. (a, b) SEM images of CTO and (c-f) their SEM-mapping images.

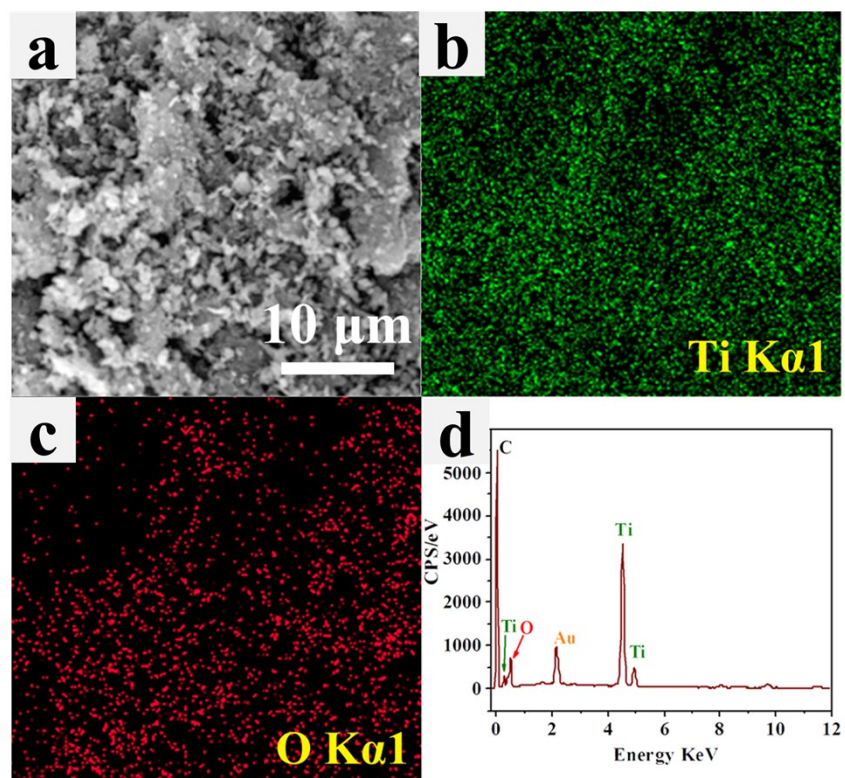


Figure S4. (a) SEM image of HTO, and (b-c) their SEM-mapping images and (d) EDX profile.

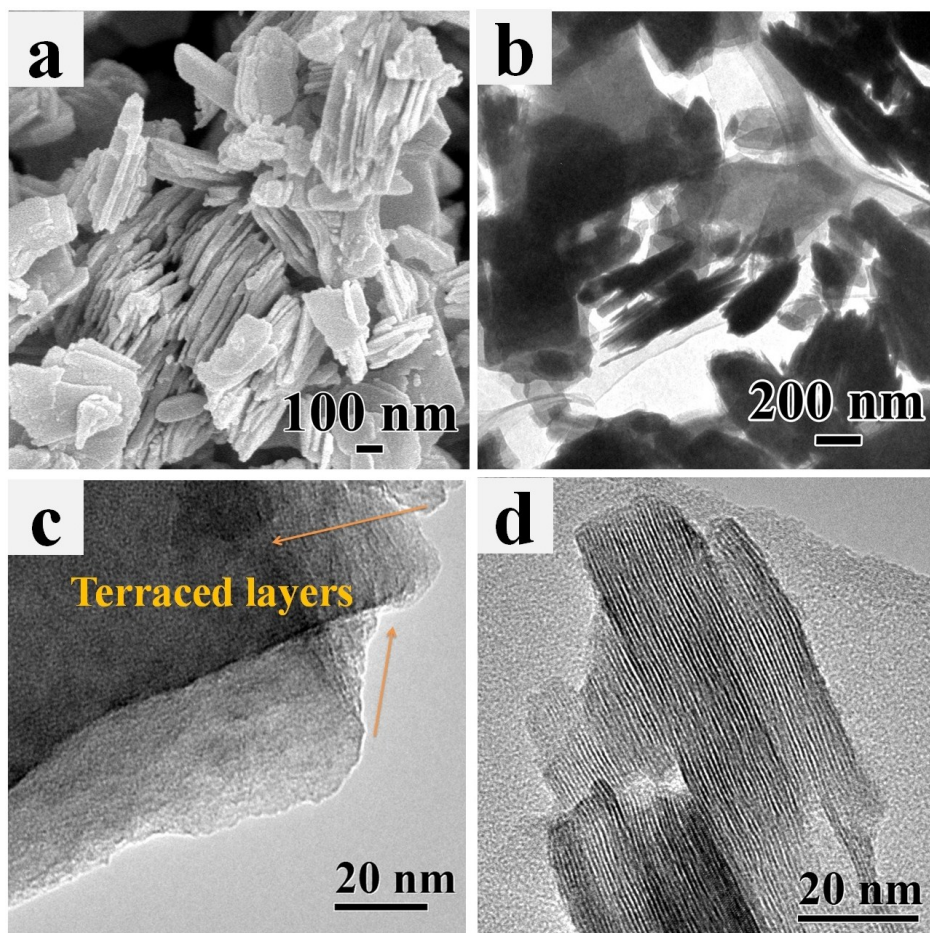


Figure S5. (a) SEM image of HTO and (b, c, d) TEM images of HTO with different visual angle.

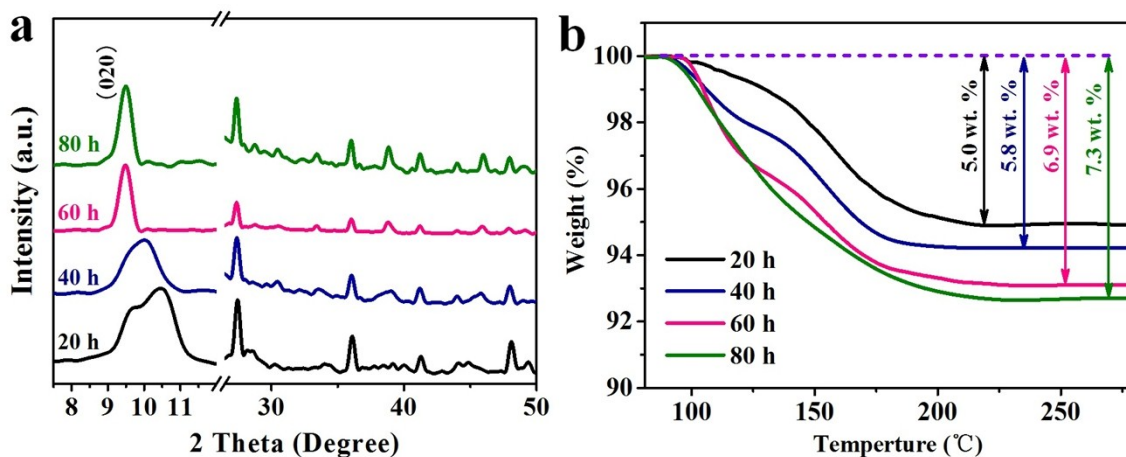


Figure S6. (a) XRD pattern of HTO with different protonation time. (b) TG curves of HTO with different protonation time to measure their water content.

We have designed different protonized degree samples *via* controlling protonation time (20, 40, 60, and 80 h). Briefly, the (020) of HTO (Figure S5a) is gradually emerged and the content of crystal water (Figure S5b) boost with the increase of protonation time. HRTEM images (Figure S6) directly confirm that lattice spacing of (020) gradually enlarge with the deeper of protonation degree. However, the flake architecture becomes thicker as well. Since the kinetics of Mg^{2+} is sluggish, the products with large layered spacing, lower water content and fewer layers number could strengthen its electrochemical performance. Discharge-charge curves (Figure S7) show that the HTO protonated for 60 h delivers the highest reversible capacity of 142 mA h g^{-1} . Therefore, the HTO protonated for 60 h with large layer spacing of 0.93 nm and 6.9 wt. % water content ($H_{0.68}Ti_{1.83}O_7 \cdot 0.64H_2O$) should be the best candidate for further study.

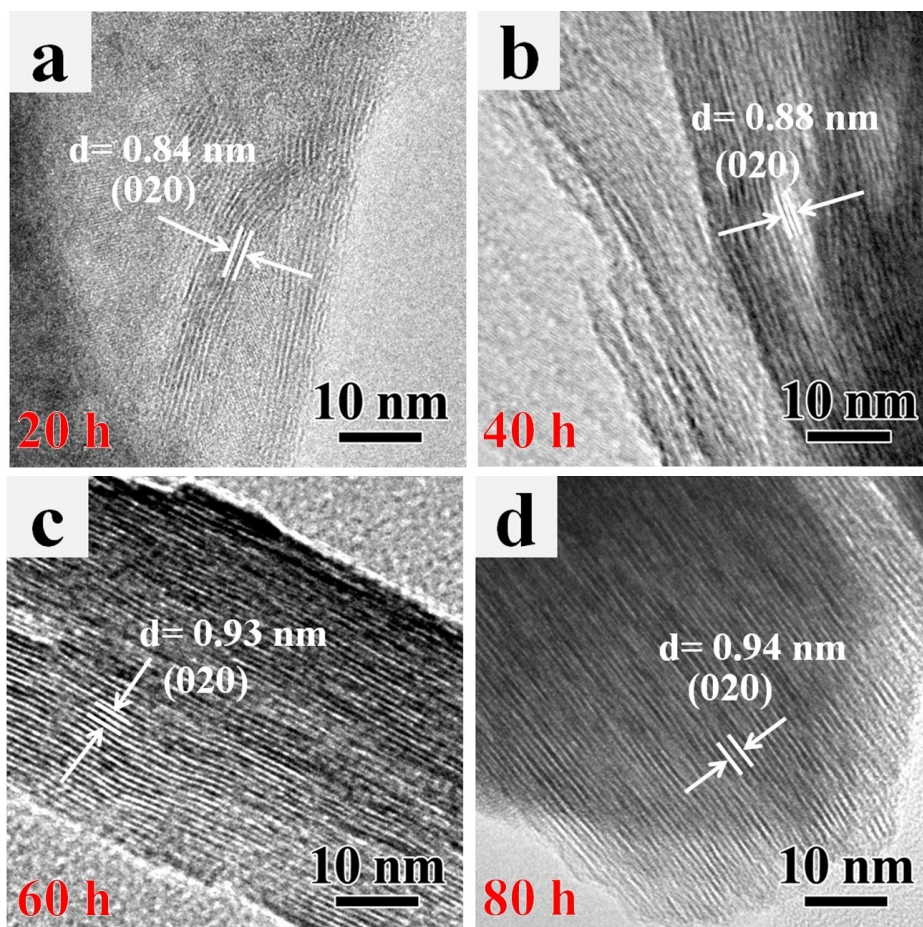


Figure S7. HRTEM images of HTO with different protonation time.

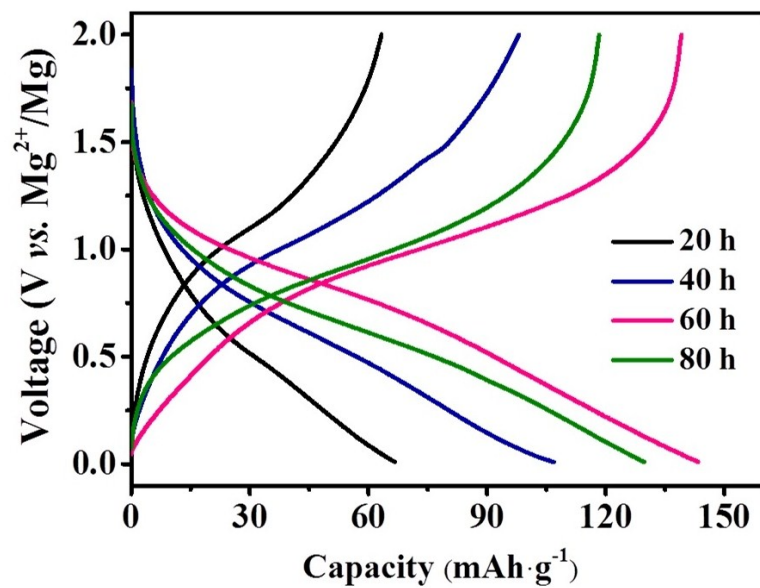


Figure S8. Discharge-charge profiles of HTO with different protonation time at current density of 50 mA g⁻¹.

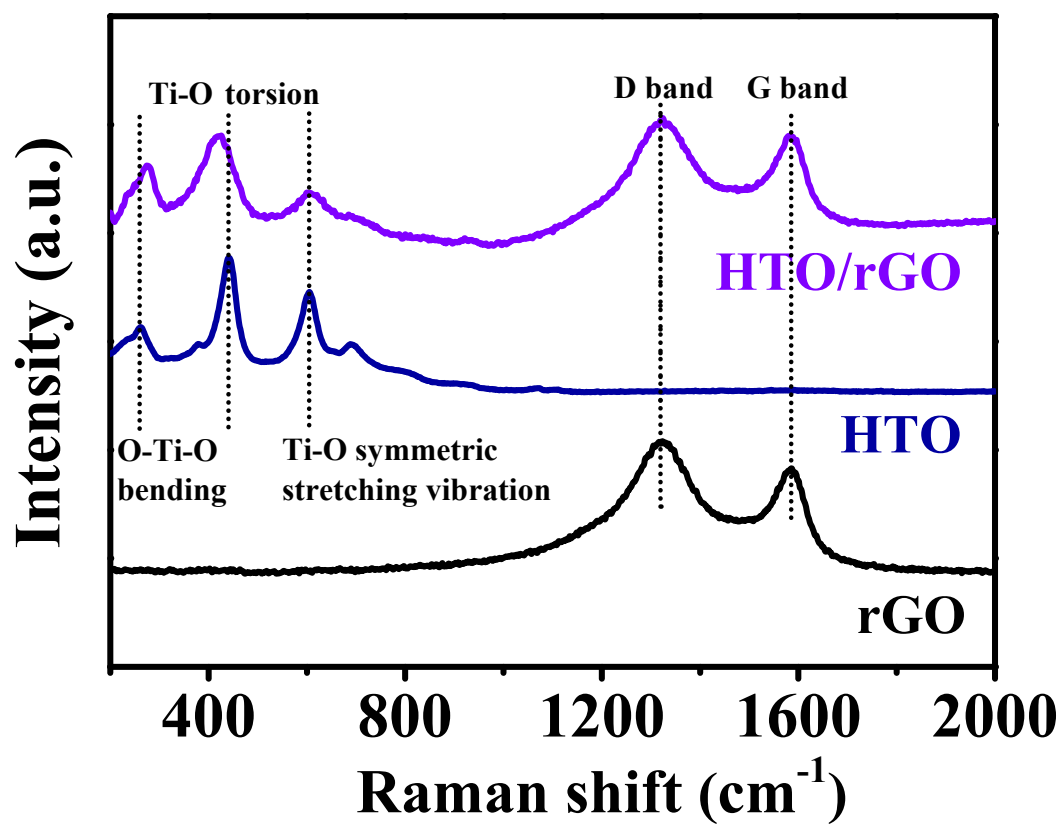


Figure S9. Raman spectra of rGO, HTO and HTO/rGO.

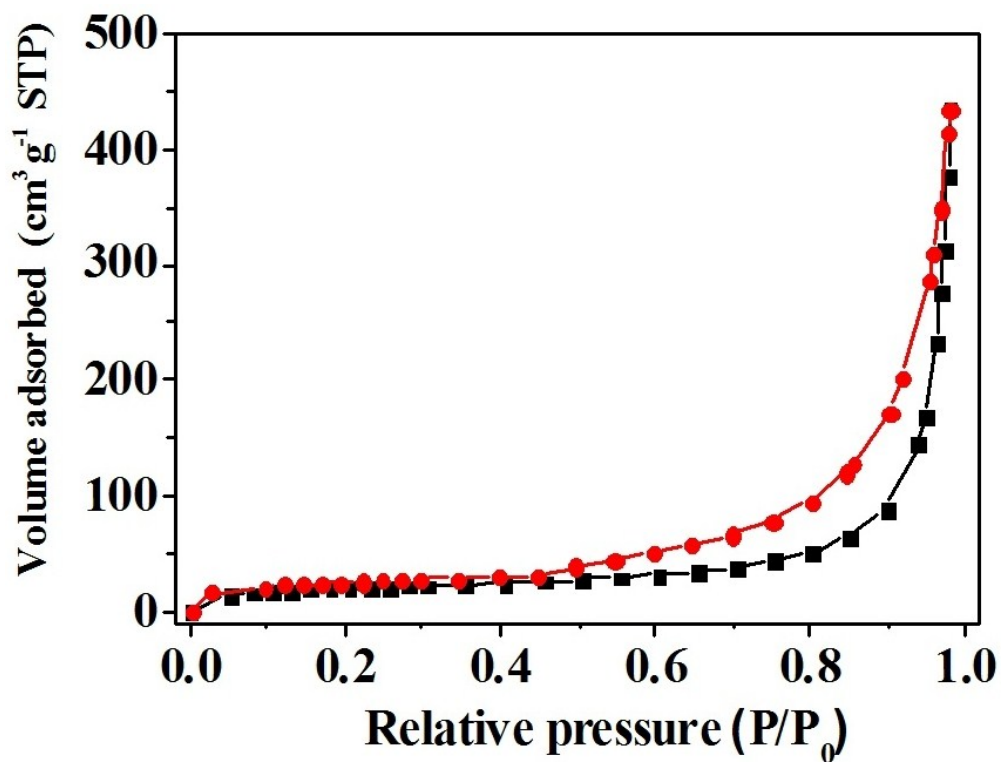


Figure S10. Nitrogen adsorption and desorption isotherm of HTO/rGO (black: nitrogen adsorption curve; red: nitrogen desorption curve).

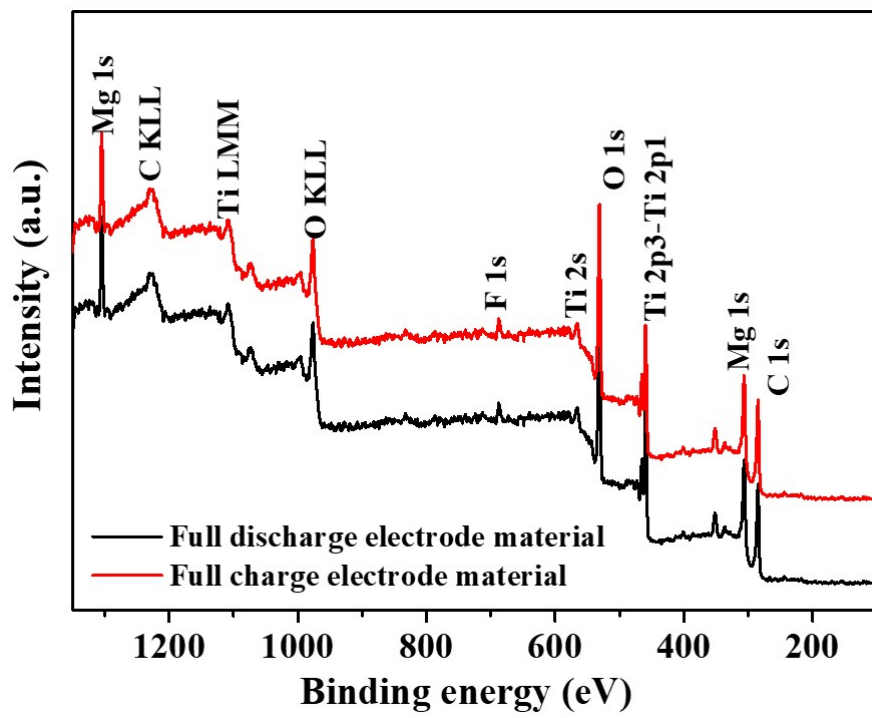


Figure S11. XPS results for fully discharged and charged electrode materials

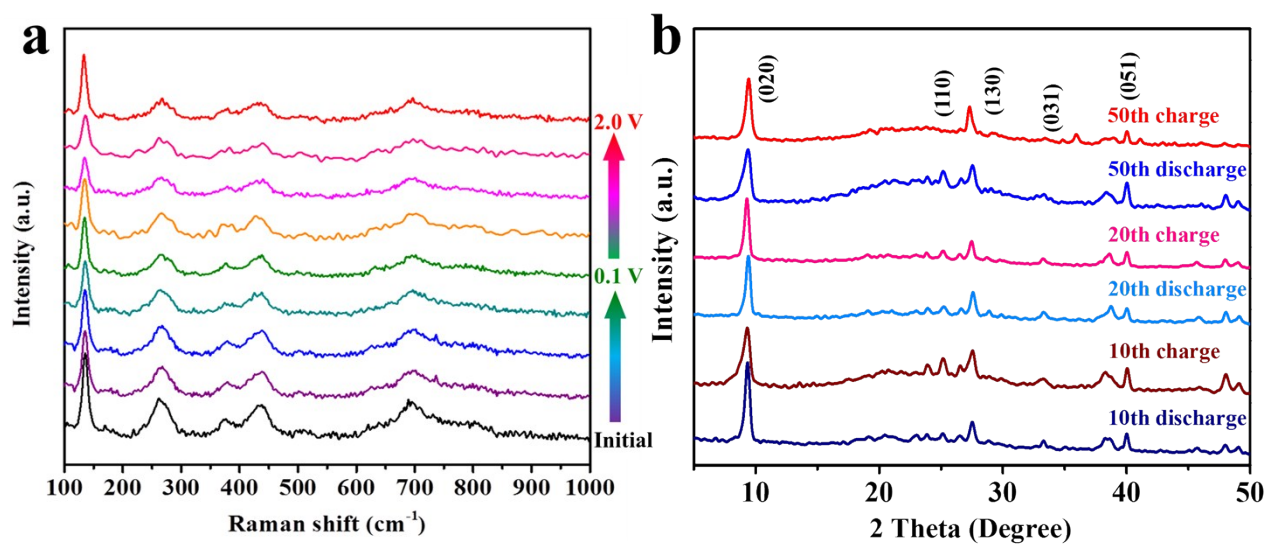


Figure S12. (a) Ex situ Raman spectrum of HTO electrode during the first cycle.

(b) XRD patterns of HTO electrodes with selected states.

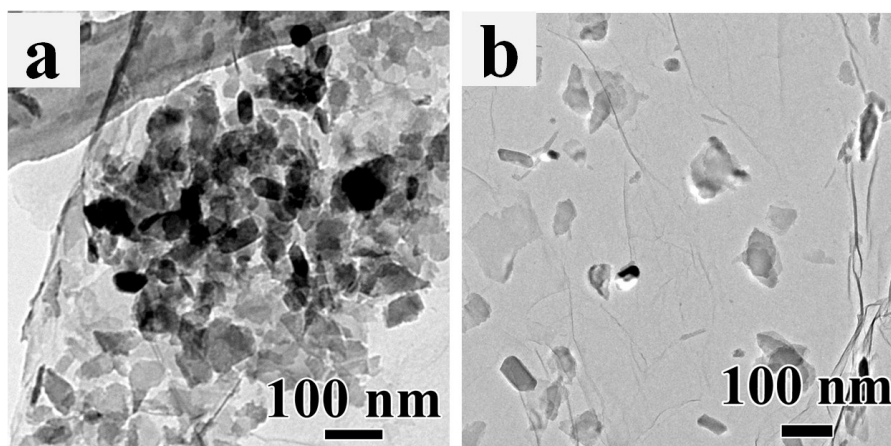


Figure S13. TEM images of HTO/rGO with different amount rGO (a) 4.5 wt. %, (c) 31.7 wt. %.

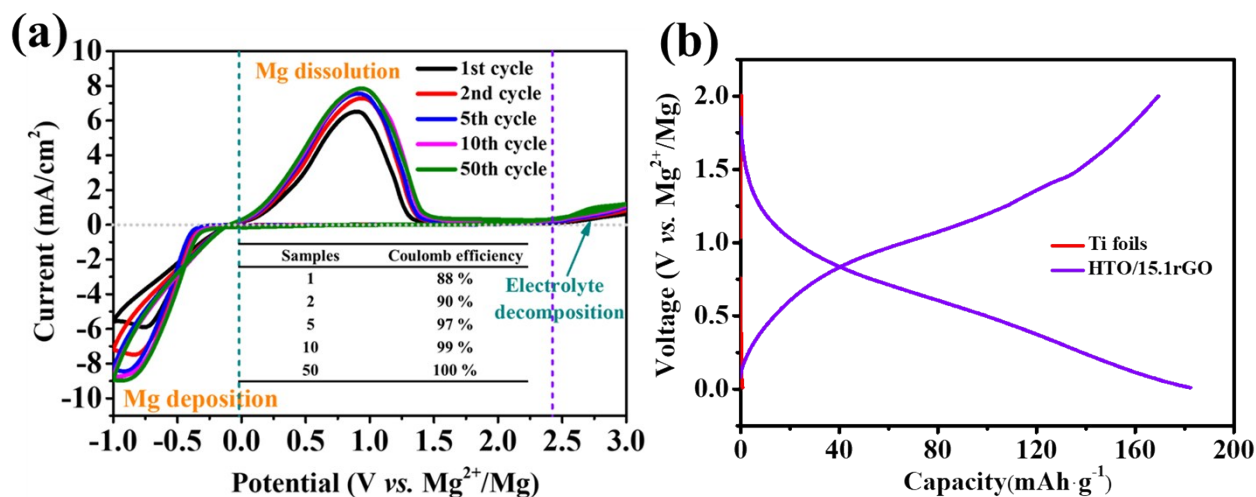


Figure S14. (a) CVs of 0.25 M APC electrolyte measured using pure Ti electrodes at 25 mV/s at selected cycles and corresponding columbic efficiency. (b) Discharge/Charge profiles of HTO/15.1rGO using Ti as current collectors and Ti electrode without active materials (Ti//0.25 M APC//Mg) at current density of 20 mA g⁻¹.

Results show the cyclic voltammograms (CVs) of APC electrolyte on Ti current collector. It reveals that APC show the remarkable deposition-dissolution property and increased Columbic efficiency within the voltage windows below 2.4 V (vs. Mg²⁺/Mg) on pure Ti electrode. Meantime, the specific capacity of the Ti electrode (Mg/Ti cell) is 0.76 μ A h cm⁻², which could be ignored compared with the capacity of active materials.

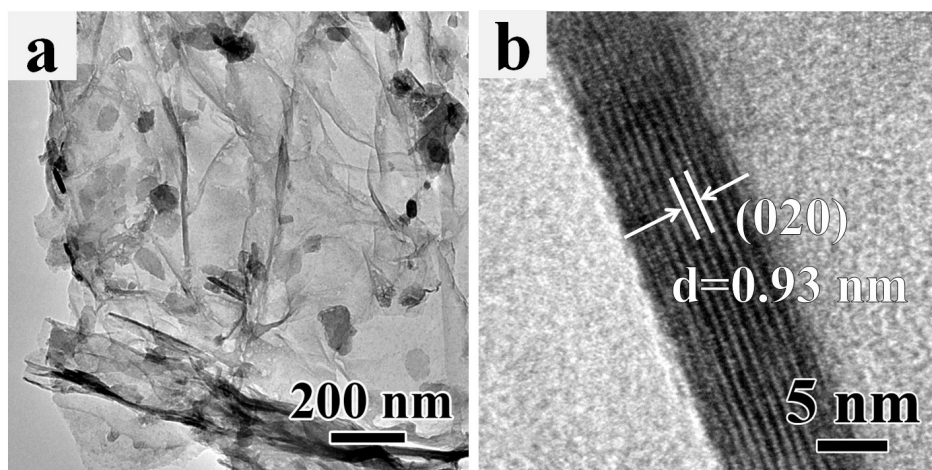


Figure S15. (a) TEM and (b) HRTEM image of HTO/15.1rGO electrodes after 100 cycles.

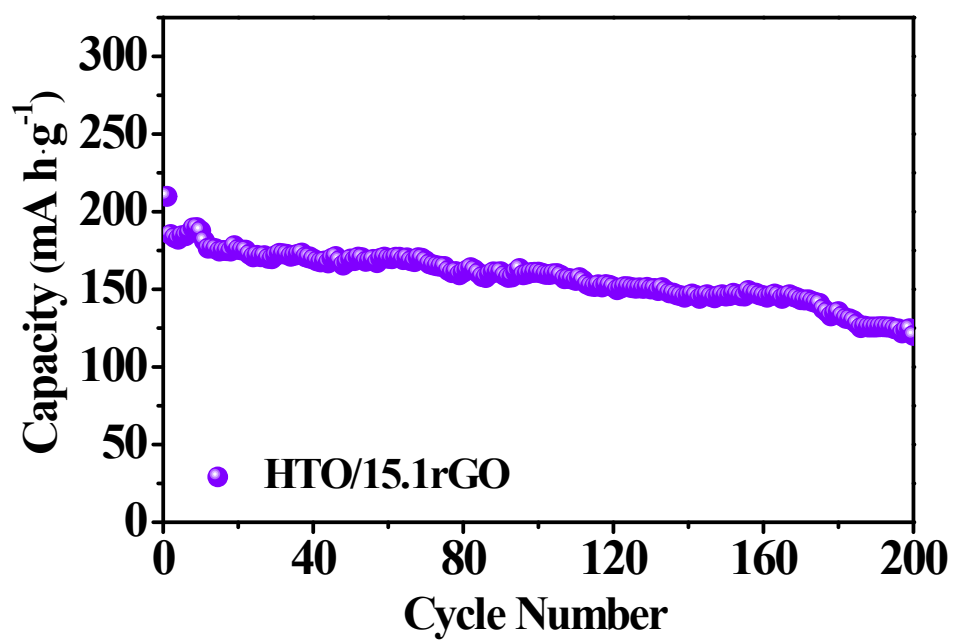


Figure S16. The long-term cycle performance HTO/15.1rGO (discharge capacity) with a current density of 50 mA g⁻¹.

Table S1. The DFT calculated parameters of $\text{H}_{0.68}\text{Ti}_{1.83}\text{O}_4$ and $\text{Mg}_{0.5}\text{Ti}_{1.83}\text{O}_4$.

Samples	a (Å)	b (Å)	c (Å)	$\alpha=\beta=\gamma$	V(Å ³)
$\text{H}_{0.68}\text{Ti}_{1.83}\text{O}_4$	3.632	18.882	3.011	90	206.5
$\text{Mg}_{0.5}\text{Ti}_{1.83}\text{O}_4$	3.902	17.410	3.038	90	206.4